CAE v2: Context Autoencoder with CLIP Latent Alignment

Anonymous authors
Paper under double-blind review

Abstract

Masked image modeling (MIM) learns visual representations by predicting the masked patches on a pre-defined target. Inspired by MVP (Wei et al., 2022b) that displays impressive gains with CLIP, in this work, we also employ the semantically rich CLIP latent as target and further tap its potential by introducing a new MIM pipeline, CAE v2, for learning a high-quality encoder and facilitating model convergence on the pre-training task. CAE v2 is an improved variant of CAE (Chen et al., 2022a), applying the CLIP latent on two pretraining tasks, *i.e.*, visible latent alignment and masked latent alignment. Visible latent alignment directly mimics the visible latent representations from the encoder to the corresponding CLIP latent, which is beneficial for facilitating model convergence and improving the representative ability of the encoder. Masked latent alignment predicts the representations of masked patches within the feature space of CLIP latent as standard MIM task does, effectively aligning the representations computed from the encoder and the regressor into the same domain. We evaluate CAE v2 on various downstream vision tasks and demonstrate that our method achieves competitive performance on image classification, semantic segmentation, object detection and instance segmentation. CAE v2 also outperforms the CLIP vision encoder on these tasks, although CAE v2 is not designed for direct comparison with CLIP. Code will be available.

1 Introduction

Masked image modeling (MIM) (Bao et al., 2022) task has attracted numerous attention in self-supervised representation learning, showing strong performance on a variety of downstream tasks. Previous MIM methods (Bao et al., 2022; He et al., 2022; Xie et al., 2022; Chen et al., 2022a) usually mask out some image patches, and then predict these masked patches conditioned on representations of visible patches according to specific prediction targets. The architecture of these MIM methods can be unified with an encoder-decoder format, in which the encoder is used for the representation learning and the decoder is used for the prediction of the masked patches. When transferring to downstream tasks, MIM only maintains the learned encoder and discards other parts.

A high-quality pre-trained encoder can greatly benefit downstream tasks. To improve the encoding quality, previous works take efforts on two aspects, *i.e.*, using better pretraining targets and decoupling the learning of encoder and decoder. As for the type of target, instead of low-level signals like RGB (He et al., 2022; Xie et al., 2022) and hand-crafted features like HOG (Wei et al., 2022a), some methods intuitively use high-level semantically rich targets to help the encoder learn more informative semantics, *e.g.*, discrete visual tokens (Bao et al., 2022; Chen et al., 2022a; El-Nouby et al., 2021; Peng et al., 2022a; Dong et al., 2021), features from momentum encoders (Tao et al., 2022; Chen et al., 2022b; Wu et al., 2023), and features from pretrained models (Wei et al., 2022b;a; Fang et al., 2023b;a; Hou et al., 2022; Peng et al., 2022b). Among these literature, MVP (Wei et al., 2022b) first utilizes CLIP latent as the masked prediction target in MIM, showing impressive gains on various downstream tasks. Another line like MAE (He et al., 2022) and CAE (Chen et al., 2022a) attempts to partition the representation learning of the encoder and the reconstruction of the masked patches. For example, CAE introduces a latent contextual regressor to explicitly decouple the encoder learning and the decoder reconstruction, which effectively motivates encoder's power.

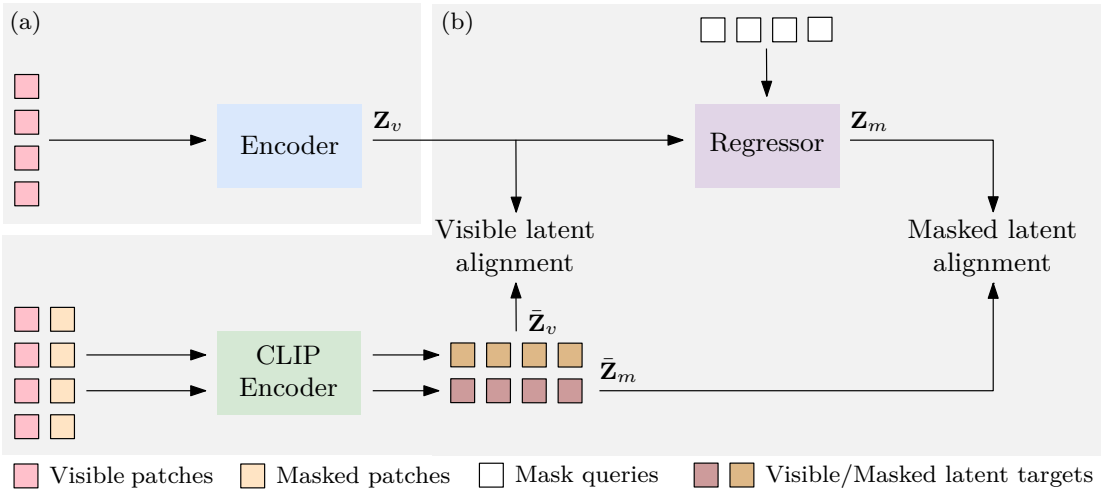

Figure 1: The pipeline of CAE v2. (a) The encoder receives the visible patches and extracts the visible latent representations $\mathbf{Z}_v$, which is then put into the regressor to generate masked latent representations $\mathbf{Z}_m$ conditioned on the mask queries. CAE v2 consists of two loss functions: visible latent alignment - mimicking $\mathbf{Z}_v$ to the visible latent targets $\bar{\mathbf{Z}}_v$, and masked latent alignment - regressing $\mathbf{Z}_m$ with the masked latent targets $\bar{\mathbf{Z}}_m$. Both $\bar{\mathbf{Z}}_v$ and $\bar{\mathbf{Z}}_m$ are generated by the vision branch of CLIP model. After pretraining, the encoder (a) is applied to downstream tasks, while (b) is replaced with the downstream task part.

In this paper, we choose CLIP latent as the pretraining target following MVP (Wei et al., 2022b), while deeply tapping the potential of CLIP latent to acquire a high-quality vision encoder. We first introduce a new MIM pipeline, termed CAE v2, which is a context autoencoder with CLIP latent alignment. The architecture of CAE v2 is built upon the CAE (Chen et al., 2022a) method, with the variation on retaining the encoder and the regressor yet discarding the decoder. It results in a more lightweight model structure, enabling faster model pretraining and less computational cost.

The key novelty of CAE v2 lies in two concurrent pretraining tasks, *i.e.*, visible latent alignment and masked latent alignment. Visible latent alignment is designed for an explicit optimization on the encoder, which imposes visible latent representations from the encoder to be close to those from the vision branch of CLIP model. This alignment encourages the encoder to learn semantically rich information brought by supervision signals directly, which is beneficial for model convergence and performance improvement. Meanwhile, masked latent alignment is responsible for the masked patch prediction. It directly regresses feature representations of the masked patches from the regressor to the corresponding CLIP latents as standard MIM methods do. These two tasks are able to align the feature representations from the encoder with those from the regressor, which also share the same feature space with CLIP latents. In this way, both encoder and regressor can be fully learned, especially on the encoder that is maintained for downstream tasks. The two latent alignment are applied as two loss functions relying on the loss type of cosine distance, even though our CAE v2 is robust to different loss types.

We also generalize our approach to a range of model scales: from the tiny size to the large size. Extensive experiments on various downstream tasks demonstrate that our CAE v2 achieves competitive results across all scales of models on image classification, semantic segmentation, object detection, and instance segmentation. In addition, due to the specialized vision representation learning, CAE v2 even achieves superior results on downstream vision tasks than the vision branch of CLIP model, which is learned for image-text alignment. In summary, our contributions are:

- We develop a new MIM pipeline, CAE v2, which is an improved version of CAE with CLIP latent as the pretraining target for learning a high-quality encoder and facilitating model convergence.
- We introduce visible latent alignment and masked latent alignment, aligning feature representations generated from the encoder and the regressor with CLIP latents.

- Experiments show that CAE v2 effectively improves the representative ability of the encoder, achieving competitive performance across model sizes and various downstream vision tasks.

2 CAE v2

CAE v2 is an improved variant of CAE (Chen et al., 2022a). Compared with CAE, CAE v2 only maintains the encoder and the regressor while discarding the decoder (as illustrated in Section 2.2). Meanwhile, CAE v2 applies two latent alignment objectives that are supervised by CLIP latents - feature representations extracted from the vision branch of CLIP (as shown in Section 2.3), which is different from CAE that uses one alignment loss and one reconstruction loss.

2.1 Preliminary: CAE

The network of CAE (Chen et al., 2022a) is an encoder-regressor-decoder architecture, including two pretraining tasks: masked representation prediction and masked patch reconstruction. The key of CAE is to decouple learning of encoder from completing the pretraining tasks, and making predictions in the encoded representation space. We illustrate the computational graph of CAE in Figure 5 (b) in Appendix.

Let $\mathbf{x} \in \mathcal{D}$ denote an input image. CAE first embeds $\mathbf{x}$ into N patches, which are then divided into two non-overlapped sets, *i.e.*, visible patches $\mathbf{X}_v$ and masked patches $\mathbf{X}_m$. Here, $N = |v| + |m|$ and $\gamma = |m| / N$, where γ represents the mask ratio. The **encoder** takes the visible patches as input and outputs visible representations $\mathbf{Z}_v$. The **regressor** then predicts the latent representations of the masked patches $\mathbf{Z}_m$ conditioned on the positions of masked patches, which are expected to be aligned with the representations $\mathbf{Z}_m$ computed from the encoder; The **decoder** then reconstructs the masked patches $\mathbf{Y}_m$ from the predicted encoded representations $\mathbf{Z}_m$ to the form of target $\bar{\mathbf{Y}}_m$. CAE includes the **reconstruction loss** for the reconstruction of masked patches, and the **alignment loss** for the alignment of features from the encoder and the regressor.

2.2 Architecture

The overview of the pipeline of CAE v2 is shown in Figure 1, and the computational graph of our CAE v2 is shown in Figure 5 (a) in Appendix. CAE v2 builds upon the foundation of CAE with two main structural modifications: without the decoder and two alignment loss functions with CLIP latent as the target. Specifically, CAE v2 is an encoder-regressor architecture, in which visible latent alignment loss is directly applied on latent representations of visible patches computed from the encoder, and masked latent alignment loss acts on latent representations of masked patches predicted from the regressor. The supervision signals of these two losses are both CLIP latents generated from the vision branch of CLIP.

Encoder. The encoder $\mathcal{F}$ only receives visible patches $\mathbf{X}_v$. It maps the visible patches $\mathbf{X}_v$ to the latent representations $\mathbf{Z}_v$ across a stack of transformer blocks that is based on self-attention. We employ a series of ViTs (Dosovitskiy et al., 2021) as the encoder, including ViT-Tiny, -Small, -Base and -Large.

Regressor. Following Chen et al. (2022a), the latent contextual regressor $\mathcal{H}$ predicts the latent representations of masked patches $\mathbf{Z}_m$ from $\mathbf{Z}_v$ conditioned on the positions of masked patches. $\mathcal{H}$ performs as the same as cross-attention, in which the queries are learnable mask tokens $\mathbf{Q}_m$, and the keys and values are both the concatenation of $\mathbf{Z}_v$ and the output of previous layers ($\mathbf{Q}_m$ for the first layer).

Decoder. The decoder is to map masked latent representations $\mathbf{Z}_m$ to the format of target $\mathbf{Y}_m$. The decoder is based on a self-attention based transformer, different from the regressor based cross-attention. Different from CAE, CAE v2 does not have the decoder, since the regressor can be responsible for predicting the latent representations of masked patches.

2.3 Objective Function

Masking. We adopt the random block-wise masking strategy as in BEiT (Bao et al., 2022). Instead of a unique mask ratio, we apply variable mask ratios for different sizes of models. In detail, we experimentally

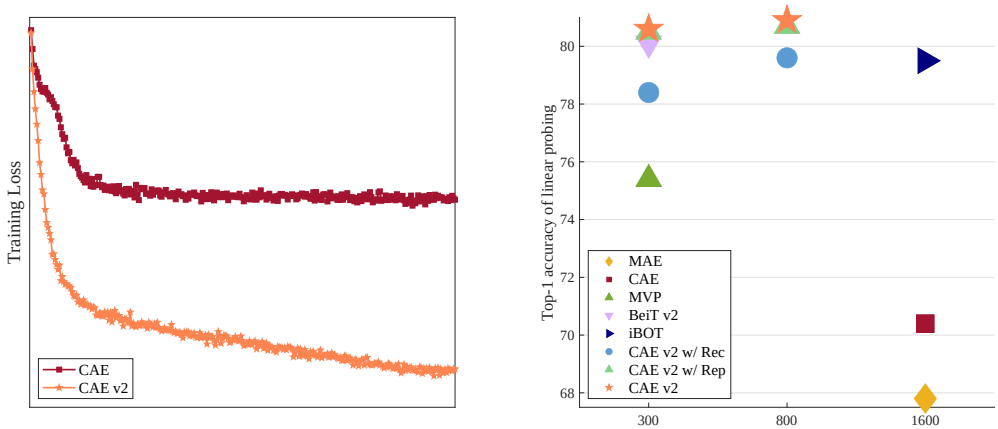

Figure 2: Analysis of the model convergence on (left) training loss and (right) top-1 accuracy of linear probing *vs.* epochs. The x-axis denotes the pretraining epoch.

find that the optimal mask ratio is positively related with the model size, *i.e.*, the larger the model, the higher the mask ratio. More analyses are provided in Section 3.2.

Targets. We utilize the vision branch of CLIP (Radford et al., 2021) model to produce CLIP latent as the pretraining target. The intact image is fed into the target model $\mathcal{T}$ to get latent representations of patches, which are then divided into the visible latent targets $\bar{\mathbf{Z}}_v$ and the masked latent targets $\bar{\mathbf{Z}}_m$.

Loss function. CAE v2 consists of two loss functions: visible latent alignment and masked latent alignment.

Visible latent alignment loss $\ell_v(\mathbf{Z}_v, \bar{\mathbf{Z}}_v)$ is conducted on the latent representations of visible patches $\mathbf{Z}_v$ from the encoder, ensuring that the encoded representations lies in the latent representation space of the visible latent targets $\bar{\mathbf{Z}}_v$ extracted from CLIP model.

Masked latent alignment loss $\ell_z(\mathbf{Z}_m, \bar{\mathbf{Z}}_m)$ allows the latent representations of masked patches $\mathbf{Z}_m$ predicted from the regressor to be close to the masked latent targets $\bar{\mathbf{Z}}_m$ that are also CLIP latents generated from CLIP model. Overall, the whole loss function is:

$$\ell = \ell_v(\mathbf{Z}_v, \bar{\mathbf{Z}}_v) + \ell_z(\mathbf{Z}_m, \bar{\mathbf{Z}}_m), \tag{1}$$

By default, we use the cosine distance loss for both $\ell_v(\mathbf{Z}_v, \bar{\mathbf{Z}}_v)$ and $\ell_z(\mathbf{Z}_m, \bar{\mathbf{Z}}_m)$. Thus, the Eq. 1 can be represented as:

$$\ell_v(\mathbf{Z}_v, \bar{\mathbf{Z}}_v) + \ell_z(\mathbf{Z}_m, \bar{\mathbf{Z}}_m) = \frac{1}{|v|}\sum_{i=1}^{|v|}(1 - \cos(\mathbf{z}_v^i, \bar{\mathbf{z}}_v^i)) + \frac{1}{|m|}\sum_{i=1}^{|m|}(1 - \cos(\mathbf{z}_m^i, \bar{\mathbf{z}}_m^i)), \tag{2}$$

where $\mathbf{z}_v^i$ and $\bar{\mathbf{z}}_v^i$ represent the latent representation from the encoder of the i-th visible patch and its corresponding CLIP latent. Similarly, $\mathbf{z}_m^i$ and $\bar{\mathbf{z}}_m^i$ represent the latent representation from the regressor of the i-th masked patch and its corresponding CLIP latent. $\cos(\mathbf{u}, \mathbf{v}) = \frac{\mathbf{u} \cdot \mathbf{v}}{\|\mathbf{u}\|\|\mathbf{v}\|}$ represents the cosine similarity of two vectors.

Differences between loss functions of CAE v2 and CAE. CAE v2's loss functions (including visible latent alignment loss and masked latent alignment loss) differ from the original CAE's loss function (including reconstruction loss and alignment loss) on: i) *Target*. CAE v2's loss functions both use CLIP latent as target, while CAE's reconstruction loss uses DALL-E and alignment loss uses latent representation from its encoder as target. ii) *Loss type*. CAE v2's loss functions both use the cosine distance loss, while CAE's reconstruction loss uses the cross-entropy loss and alignment loss uses the MSE loss. iii) *Manner*. CAE v2's loss functions directly optimize the encoder with visible latent alignment loss and the regressor with masked latent alignment loss, which encourages the encoder to be fast and fully learned. In contrast, CAE's reconstruction loss is applied on the decoder and alignment loss is used to align the representations from its regressor and its encoder, thus the encoder's learning is slow and implicit. These three differences on

Table 1: Individual change from CAE to CAE v2. l_v and l_z represent visible and masked latent alignment. The backbone is ViT-Base. All models are pre-trained for 300 epochs.

No.	Method	IN-1K		ADE20K	Object detection & instance segmentation	
		LIN	FT	mIoU	Mask R-CNN	Cascade Mask R-CNN
0	CAE	64.1	83.6	48.3	48.4 & 42.6	51.6 & 44.6
1	+ CLIP (baseline)	75.8	83.6	49.5	49.3 & 43.0	51.7 & 44.6
2	+ l_z	78.4	85.0	52.7	51.8 & 44.3	53.8 & 45.8
3	+ l_v (CAE v2)	**80.7**	**85.5**	**53.4**	**52.4** & **45.3**	**54.2** & **46.5**

loss functions help our CAE v2 learn a better encoder than CAE. It can be verified on the linear probing downstream task that CAE v2 is superior than CAE by +10.3% (as shown in Table 6).

Study and discussion. Different from previous MIM works, CAE v2 directly optimizes the encoder with visible latent alignment loss ℓ_v on representations of the visible patches. Since supervision signals come from a semantically rich CLIP model, this loss can effectively facilitate the model convergence. It can be verified by Figure 2 that with 300-epoch pretraining schedule, the model with only using ℓ_v already achieves remarkable performance, which is largely superior than only using masked alignment loss ℓ_z. When expending the pretraining schedule to 800 epoch, the gap between only using ℓ_v and only using ℓ_z reduces, showing that ℓ_v is good for the model convergence. Besides, the superior performance of only using ℓ_v on the linear probing task indicates that the representative ability of the encoder improves. The underlying reason is that ℓ_v successfully encourages the encoder to focus on the representation learning, instead of diverting some efforts to the masked patch prediction task. Consequently, the visible latent alignment plays an essential role in MIM pretraining task. Meanwhile, only using ℓ_z also achieves comparable performance. Even on the high performance of only using ℓ_v, ℓ_z can further improves the performance, showing that it is effective to align the encoder and the decoder to the same feature space.

3 Experiments

3.1 Settings

Baseline. The baseline of CAE v2 is replacing CAE's target to CLIP latent (as shown in No.1 in Table 1).

Model structures. We study a series of vision transformer backbones (Dosovitskiy et al., 2021), including ViT-Tiny (12 layers with *dim*=192), ViT-Small (12 layers with *dim*=384), ViT-Base (12 layers with *dim*=768), and ViT-Large (24 layers with *dim*=1024). Note that for ViT-Tiny, we follow Wang et al. (2022) to increase the number of heads from 3 to 12, which gives better results on ImageNet-1K (Deng et al., 2009). For other models, we strictly follow the model configurations as in Dosovitskiy et al. (2021).

For the target model, we adopt the vision branch CLIP-Base/16 of CLIP[1] for the pretraining experiments with ViT-Tiny/-Small/-Base and CLIP-Large/14 for ViT-Large. The size of input images is 224×224 for CLIP-Base/16 and 196×196 for CLIP-Large/14.

Pretraining. Following most previous MIM methods (Bao et al., 2022; He et al., 2022; Chen et al., 2022a; Wei et al., 2022b; Wang et al., 2022), we use ImageNet-1K (IN-1K) dataset (Deng et al., 2009) for all pretraining experiments. The input images are with the size of 224×224 and are partitioned into 14×14 patches with the patch size being 16×16 across all sizes of models. We apply random resized cropping and horizontal flipping during pretraining.

The default mask ratios in the pretraining stage are set to 15%, 25%, 50%, and 60% on ViT-Tiny, -Small, -Base, and -Large, respectively. Without clear specification, we use AdamW (Loshchilov & Hutter, 2019) for optimization and train CAE v2 for 300 epochs across all scales of ViTs (Dosovitskiy et al., 2021). More detailed settings are listed in the appendix.

Evaluation. We evaluate our CAE v2 on various downstream tasks. For image classification, we conduct evaluations on ImageNet-1K (Deng et al., 2009) with both linear probing (LIN) and fine-tuning (FT) proto-

[1]The official pretrained CLIP model is available at `https://github.com/openai/CLIP/blob/main/clip/clip.py`.

Table 2: Effectiveness of visible latent alignment loss ℓ_v and masked latent alignment loss ℓ_z in our CAE v2. All models are pre-trained for 300 epochs. Default settings are marked in gray.

Model	Loss function		IN-1K		ADE20K
	ℓ_z	ℓ_v	LIN	FT	mIoU
ViT-Tiny	✓	-	64.9	77.2	44.1
	-	✓	68.8	77.4	44.2
	✓	✓	**69.3**	**77.8**	**44.7**
ViT-Small	✓	-	73.9	82.4	49.6
	-	✓	77.3	82.8	49.6
	✓	✓	**77.5**	**83.1**	**49.8**
ViT-Base	✓	-	78.4	85.0	52.7
	-	✓	80.5	85.2	53.1
	✓	✓	**80.7**	**85.5**	**53.4**

Table 3: Ablation studies for the type of loss function in CAE v2. Both ℓ_v and ℓ_z are used and all models are pre-trained for 300 epochs. We use the cosine distance as the default loss function (marked in gray).

Model	Type of loss	IN-1K		ADE20K
		LIN	FT	mIoU
ViT-Tiny	MSE	69.1	77.3	**44.8**
	Smooth-$l1$	**69.4**	77.6	43.7
	Cosine distance	69.3	**77.8**	44.7
ViT-Small	MSE	77.3	82.7	49.8
	Smooth-$l1$	77.4	82.8	49.8
	Cosine distance	**77.5**	**83.1**	**49.8**
ViT-Base	MSE	80.4	85.3	52.9
	Smooth-$l1$	80.5	85.2	52.0
	Cosine distance	**80.7**	**85.5**	**53.4**

cols. For semantic segmentation, we follow BEiT (Bao et al., 2022) to use UperNet (Xiao et al., 2018) and report the mIoU on ADE20K (Zhou et al., 2017) dataset. For objection detection and instance segmentation, we use COCO (Lin et al., 2014) as the evaluation dataset. We adopt both Mask R-CNN (He et al., 2017) and Cascade Mask R-CNN (Cai & Vasconcelos, 2018) frameworks and report AP^b and AP^m on the COCO val split. Please refer to the appendix for more training details on various downstream tasks.

3.2 Ablation Studies

In this subsection, we first illustrate individual change from CAE to CAE v2, and then analyse the effectiveness of visible latent alignment loss and masked latent alignment loss. After that we investigate mask ratio, type of loss, layer number of the regressor, and masking sampling strategy. Details are provided below.

Individual change from CAE to CAE v2. We experiment on each individual change from CAE to CAE v2 in Table 1. i) *CLIP latent as target.* We first change CAE's target from Dall-E to CLIP. Compared with CAE, this setting improves the performance, *e.g.*, +11.5%, 1.2% and 0.9% on ImageNet-1k's linear probing, ADE20K and COCO object detection, showing that CLIP latent as target can improve the representation ability of the encoder. This setting can be seen as our **baseline**. ii) *Masked latent alignment.* We then change the loss function to the proposed masked latent alignment. The performance is further improved by +2.6%, 1.4%, 3.2%, 2.5% on ImageNet-1k's linear probing, ImageNet-1k's fine-tuning, ADE20K, COCO object detection, respectively. It verifies the effectiveness of masked latent alignment. iii) *Visible latent alignment.* We further add the proposed visible latent alignment to directly optimize the encoder. The results are further increased by +2.3%, 0.5%, 0.7% and 0.6%, demonstrating the effectiveness of visible latent alignment.

Visible latent alignment loss *vs.* masked latent alignment loss. Previous MIM methods (Bao et al., 2022; He et al., 2022; Peng et al., 2022b; Liu et al., 2022b; Chen et al., 2022a) typically apply the loss function on the predicted masked patches, as illustrated in Figure 5. Differently, CAE v2 applies two alignment losses on latent representations, *i.e.*, visible latent alignment loss ℓ_v on the representations of visible patches from the encoder, and masked latent alignment loss ℓ_z on the representations of predicted masked patches from the regressor. These two losses are independent that can be used either both of them or any individual one.

Table 2 shows the ablation results. One can see that the proposed ℓ_v and ℓ_y (*i.e.*, the main idea of CAE v2) can steadily improve the performance compared to the baseline (*i.e.*, No.1 in Table 1). Specially, CAE v2 only with ℓ_y outperforms the baseline by large margins (*e.g.*, +2.6% on linear probing), showing the important role of masked latent alignment. Meanwhile, only using ℓ_v outperforms the strategy of only utilizing ℓ_z, which verifies that the direct optimization on the encoder is beneficial for enhancing the encoder's representative quality. Combining ℓ_y with ℓ_v can achieve the best performance. Note that although the encoder is subject to the implicit influences from the masked patch prediction task to some extent, CAE v2 can still ensure a good optimization on the encoder, since the encoder directly receives supervision signals from the semantically rich CLIP model.

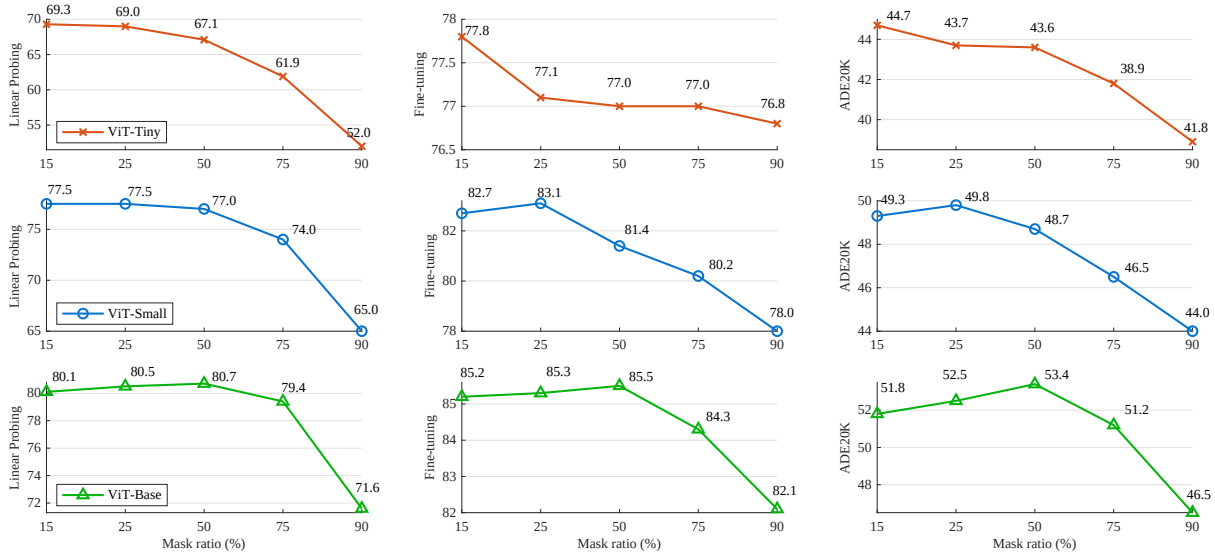

Figure 3: The optimal mask ratio is positive correlation with the model size in CAE v2. From top to bottom, the table shows the linear probing (left column), fine-tuning (middle column) on ImageNet-1K, and semantic segmentation (right column) on ADE20K with ViT-Tiny, -Small, and -Base model.

Mask ratio. We conduct experiments to analyse the influence of mask ratio, ranging from {15%, 25%, 50%, 75%, 90%}, across different scales of models. The results are listed in Figure 3. It shows that different scales of models prefer different values of mask ratios. The optimal mask ratio exhibits a positive correlation with the model size, *i.e.*, as the model size increases, a higher mask ratio performs better, and conversely, a smaller model benefits from a lower mask ratio. We also observe that when the mask ratio exceeds a stable value, the performances declines rapidly. The underlying reason might be that it is challenging for small-sized models to predict the masked patches from a limited subset of patches where most contextual information is missing. Therefore, using more visible patches can reduce the difficulty of the masked prediction task, benefiting for the model convergence. In contrast, large-scale models are easily subject to over-fitting when learning representations from overabundant visible patches, and thus a high mask ratio can make the masked prediction task more challenging to effectively mitigate the over-fitting problem. We set a mask ratio of 15%/25%/50%/60% for ViT-Tiny/-Small/-Base/-Large in our work unless specified.

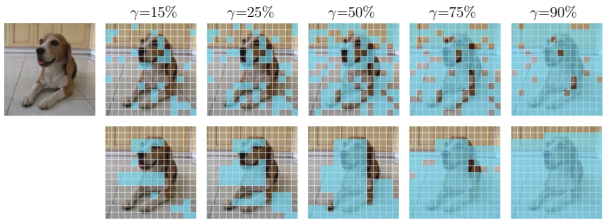

Figure 4: Illustration of corrupted images with different mask ratios γ via the random sampling strategy (top row) and the block-wise sampling strategy (bottom row). We use the block-wise sampling strategy by default.

Type of loss. We use cosine distance loss as illustrated in Eq. 2 for both visible and masked latent alignment loss functions. Instead of the cosine distance, it is possible to use other types of loss, like smooth-$\ell 1$ and mean square error (MSE), which are studied and utilized in previous works (Peng et al., 2022a; Liu et al., 2022b; Wei et al., 2022c). Therefore, we presents the results of three kinds of loss types when using latent and masked alignment simultaneously in Table 3. The results show whatever the loss type is, our CAE v2 can consistently outperform the baseline, while the cosine distance is slightly better than other types (*e.g.*, $\leq$0.5% on linear probing and fine-tuning tasks). As previous works do (*e.g.*, MASKDISTILL (Peng et al., 2022b)), we choose the optimal loss type for CAE v2, *i.e.*, cosine distance by default.

 # layers in the regressor. We tried four choices, *i.e.*, {0-layer, 1-layer, 4-layer, 8-layer}, for the number of layers in the latent contextual regressor. The results in the linear probing and the fine-tuning in Table 4 show that the effect of the layer number is minor. In contrast, the decoder depth in MAE (He et al., 2022) has a large impact on downstream tasks, especially linear probing. We conjecture that our CAE v2 benefits from the explicit visible latent alignment on the visible patches, ensuring the representative quality of the

Table 4: The influence of the layer number of the regressor in CAE v2 and the decoder depth in MAE (He et al., 2022). Models are pre-trained for 300 epochs in CAE v2 and 800 epochs in MAE. Gray represents the default setting.

Method	Model	# Layer	IN-1K	
			LIN	FT
MAE	ViT-Large	1	65.5	84.8
		4	71.9	84.9
		8	73.5	84.9
CAE v2	ViT-Base	0	80.5	85.2
		1	80.6	85.3
		4	**80.7**	**85.5**
		8	80.5	85.4

Table 5: Ablation studies for the mask sampling strategy in our CAE v2. All models are pre-trained for 300 epochs. We use the block-wise sampling by default (marked in gray).

Model	Mask strategy	IN-1K		ADE20K
		LIN	FT	mIoU
ViT-Tiny	Random	69.1	77.4	43.8
	Blockwise	**69.3**	**77.8**	**44.7**
ViT-Small	Random	77.4	82.7	49.0
	Blockwise	**77.5**	**83.1**	**49.8**
ViT-Base	Random	80.6	85.4	52.4
	Blockwise	**80.7**	**85.5**	**53.4**

encoder. When the regressor depth is 0, CAE v2 reduces to only using visible latent alignment loss, which still achieves satisfactory performance, indicating the effectiveness of visible latent alignment. We empirically use 4-layer regressor for ViT-Base/-Large and 1-layer regressor for ViT-Tiny/-Small by default.

Mask sampling strategy. We also compare different mask sampling strategies in our CAE v2, *i.e.*, the random sampling (He et al., 2022) and the block-wise sampling (Bao et al., 2022; Chen et al., 2022a; Wei et al., 2022b) (as illustrated in Figure 4). Table 5 shows that there are only approximately 0.1% gaps between these two sampling strategies on linear probing and fine-tuning, but the block-wise sampling demonstrates superior performance than the random sampling on semantic segmentation (*e.g.*, 53.4% *vs.* 52.4% on ViT-Base). We use the block-wise sampling strategy as the default option.

3.3 Main Results

Image classification on ImageNet-1K. Table 6 shows comparisons of different models using two evaluation methods: linear probing and fine-tuning.

In linear probing on ImageNet-1K, CAE v2 demonstrates significant improvements over previous methods with other targets, *e.g.*, BEiT (Bao et al., 2022), MAE (He et al., 2022), CAE (Chen et al., 2022a), and MaskFeat (Wei et al., 2022a). These gains are expected, as CLIP latents contain rich semantics than other targets. Compared to methods using CLIP latent as the target (MVP (Wei et al., 2022b) and MILAN (Hou et al., 2022)), CAE v2 also achieves superior performance (on ViT-Base with 300 epoch pretraining, CAE v2 *vs.* MVP: 80.7% *vs.* 75.4% and CAE v2 *vs.* MILAN: 80.7% *vs.* 78.9%).

In the fine-tuning task on ImageNet-1K, CAE v2 also achieves comparable performance across all scales of ViTs. Specifically, CAE v2 achieves **85.5%** top-1 accuracy with ViT-Base, surpassing all prior methods except for dBOT (Liu et al., 2022b). Note that dBOT only outperforms CAE v2 by 0.2% while requiring 1600 epochs for pretraining, demonstrating CAE v2's higher efficiency.

Semantic segmentation on ADE20K. Semantic segmentation is a challenging task that needs to classify every pixel in an image according to various semantic labels. CLIP (Radford et al., 2021) latent serves as a powerful target for this task, showing clear advantages. As shown in Table 6, CAE v2 significantly outperforms methods pre-trained with other targets, *e.g.*, 3.2% mIoU improvement over CAE (Chen et al., 2022a) when using ViT-Base. In comparison to MVP (Wei et al., 2022b) and BEIT V2 (Peng et al., 2022a), CAE v2 surpasses them with the same or less pretraining epochs. The superior performance persists when transitioning to ViT-Large, with which CAE v2 achieves **57.9%** mIoU on ADE20K (Zhou et al., 2017), outperforming previous methods.

Object detection and instance segmentation on COCO. We evaluate the pre-trained models on COCO (Lin et al., 2014) with Mask R-CNN (He et al., 2017) and Cascade Mask R-CNN (Cai & Vasconcelos, 2018; He et al., 2017) in Table 7. We report the results for 1× (12 epochs) training schedule. Compared with other pretraining methods, CAE v2 excels at both two configurations. With Mask R-CNN, CAE v2 achieves a 4.9% increase with ViT-Small and 2.4% increase with ViT-Base on AP^b compared to previous best method Chen et al. (2022a). The superior performance is maintained when employing Cascade Mask

Table 6: pretraining evaluation on the top-1 accuracy (%) on linear probing (LIN) and fine-tuning (FT) on ImageNet-1K (Deng et al., 2009), and mIoU (%) on semantic segmentation on ADE20K (Zhou et al., 2017). ‡ means our implementation using the officially released code. § means the results from Chen et al. (2022a) and Wei et al. (2022c). All other results except for ours are from the original papers. The methods achieving the best, second best and third place performance are denoted in **bold red**, green and blue respectively.

Methods	#Epochs	Target	IN-1K		ADE20K
			LIN	FT	mIoU
Methods using ViT-Tiny:					
MAE-Tiny (Wang et al., 2022)	400	RGB	23.4	76.2	-
CAE (Chen et al., 2022a)‡	300	DALL-E	28.1	75.9	38.3
Distilled MAE-lite (Wang et al., 2022)	400	RGB	-	76.5	-
G2SD (Wei et al., 2023)	200	MAE-Base	-	77.0	44.5
CAE v2	300	CLIP-Base	**69.3**	**77.8**	**44.7**
Methods using ViT-Small:					
MoCo v3 (Chen et al., 2021)§	300	Self-EMA	73.1	81.7	-
BEiT (Bao et al., 2022)§	300	DALL-E	15.7	81.7	-
SplitMask (El-Nouby et al., 2021)	300	DALL-E	-	81.5	-
CAE (Chen et al., 2022a)	300	DALL-E	51.8	82.0	-
iBOT (Zhou et al., 2022a)	3200	Self-EMA	**77.9**	82.3	45.4
G2SD (Wei et al., 2023)	200	MAE-Base	-	82.5	48.0
CAE v2	300	CLIP-Base	77.5	**83.1**	**49.8**
Methods using ViT-Base:					
MoCo v3 (Chen et al., 2021)	300	Self-EMA	76.5	83.2	47.2
DINO (Caron et al., 2021)§	400	Self-EMA	77.3	83.3	47.2
iBOT (Zhou et al., 2022a)	1600	Self-EMA	79.5	84.0	50.0
BEiT (Bao et al., 2022)	800	DALL-E	56.7	83.2	45.6
SimMIM (Xie et al., 2022)	800	RGB	56.7	83.8	-
MAE (He et al., 2022)	1600	RGB	68.0	83.6	48.1
CAE (Chen et al., 2022a)	1600	DALL-E	70.4	83.9	50.2
SdAE (Chen et al., 2022b)	300	Self-EMA	64.9	84.1	48.6
SIM (Tao et al., 2022)	1600	Self-EMA	76.4	83.8	-
MaskFeat (Wei et al., 2022a)	1600	HOG	-	84.0	-
SplitMask (El-Nouby et al., 2021)	300	DALL-E	-	83.6	45.7
PeCo (Dong et al., 2021)	800	VQGAN	-	84.5	48.5
data2vec (Baevski et al., 2022)	800	Self-EMA	-	84.2	-
CMAE (Huang et al., 2022b)	1600	RGB	-	84.7	50.1
ExtreMA (Wu et al., 2023)	300	Self-EMA	73.3	83.7	47.9
CLIP (Radford et al., 2021)	-	Text	80.2	84.9	51.1
MaskCLIP (Dong et al., 2023)	1600	Text	72.9	84.1	50.8
MVP (Wei et al., 2022b)	300	CLIP-Base	75.4	84.4	52.4
FD-CLIP (Wei et al., 2022c)	300	CLIP-Base	80.3	84.9	52.8
MILAN (Hou et al., 2022)	400	CLIP-Base	78.9	85.4	52.7
BEIT V2 (Peng et al., 2022a)	1600	VQ-CLIP-Base	-	85.5	53.1
dBOT (Liu et al., 2022b)	1600	CLIP-Base	–	**85.7**	52.9
MASKDISTILL (Peng et al., 2022b)	300	CLIP-Base	–	85.0	**53.8**
CAE v2	300	CLIP-Base	**80.7**	85.5	53.4
Methods using ViT-Large:					
MoCo v3 (Chen et al., 2021)§	300	Self-EMA	-	84.1	49.1
BEiT (Bao et al., 2022)§	1600	DALL-E	-	85.2	53.3
iBOT (Zhou et al., 2022a)	1200	Self-EMA	81.0	84.8	-
MAE (He et al., 2022)	1600	RGB	75.8	85.9	53.6
CAE (Chen et al., 2022a)	1600	DALL-E	78.1	86.3	54.7
data2vec (Baevski et al., 2022)	1600	Self-EMA	-	86.6	-
CLIP (Radford et al., 2021)§	-	Text	83.5	86.1	53.5
MVP (Wei et al., 2022b)	300	CLIP-Base	-	86.3	54.3
BEIT V2 (Peng et al., 2022a)	1600	VQ-CLIP-Base	-	87.3	56.7
FD-CLIP (Wei et al., 2022c)	300	CLIP-Large	**84.8**	87.7	55.7
MILAN (Hou et al., 2022)	400	CLIP-Large	84.3	**87.8**	**57.9**
dBOT (Liu et al., 2022b)	1600	CLIP-Large	–	**87.8**	56.2
MASKDISTILL (Peng et al., 2022b)	300	CLIP-Large	–	87.6	**57.9**
CAE v2	300	CLIP-Large	84.4	87.6	**57.9**

Table 7: pretraining evaluation on object detection (DET) and instance segmentation (INS) on COCO (Lin et al., 2014) with Mask R-CNN (He et al., 2017) (left) and Cascade Mask R-CNN (Cai & Vasconcelos, 2018) (right). All experiments are trained with the 1× schedule (12 epoch). Results except for CAE v2 are from Chen et al. (2022a) and Liu et al. (2022b). #Epochs refers to the pretraining epochs on ImageNet-1K. * denotes multi-crop pretraining augmentation. The methods achieving the best and second best performance are denoted in **bold red** and green respectively.

Method	#Epochs	Mask R-CNN		Cascade Mask R-CNN	
		DET	INS	DET	INS
		AP^b	AP^m	AP^b	AP^m
Methods using ViT-Small:					
DeiT (Touvron et al., 2021)	300	43.1	38.4	-	-
MoCo v3* (Chen et al., 2021)	300	43.3	38.8	-	-
BEiT (Bao et al., 2022)	300	35.6	32.6	-	-
CAE (Chen et al., 2022a)	300	44.1	39.2	-	-
iBOT* (Zhou et al., 2022a)	3200	-	-	49.4	42.6
CAE v2	300	**49.0**	**42.2**	**51.5**	**43.9**
Methods using ViT-Base:					
DeiT (Touvron et al., 2021)	300	46.9	41.5	-	-
MoCo v3* (Chen et al., 2021)	300	45.5	40.5	-	-
DINO* (Caron et al., 2021)	400	46.8	41.5	-	-
BEiT (Bao et al., 2022)	800	42.1	37.8	-	-
MAE (He et al., 2022)	1600	48.4	42.6	51.3	44.3
data2vec (Baevski et al., 2022)	800	41.1	37.0	-	-
iBoT (Zhou et al., 2022a)	1600	48.6	43.1	51.2	44.2
CAE (Chen et al., 2022a)	1600	50.0	44.0	52.9	45.5
dBoT (Liu et al., 2022b)	1600	-	-	53.6	-
CAE v2	300	**52.4**	**45.3**	**54.2**	**46.5**
Methods using ViT-Large:					
MAE (He et al., 2022)	1600	54.0	47.1	-	-
data2vec (Baevski et al., 2022)	1600	46.1	41.0	-	-
iBoT (Zhou et al., 2022a)	1600	50.6	44.7	-	-
CAE (Chen et al., 2022a)	1600	54.5	**47.6**	-	-
dBoT (Liu et al., 2022b)	1600	-	-	56.8	-
CAE v2	300	**55.2**	47.3	**56.9**	**48.6**

R-CNN as the fine-tuned model. For example, CAE v2 achieves a 0.6% increase with ViT-Base and 0.1% increase with ViT-Large on AP^b compared to Liu et al. (2022b).

Compared with related works (*e.g.*, MASKDISTILL (Peng et al., 2022b) and MVP (Wei et al., 2022b)) that also utilize CLIP latent as target, the performance gap may be caused by: i) architecture choices. CAE v2 is built upon CAE (Chen et al., 2022a) with structural modifications, while MASKDISTILL and MVP are based on BEiT Bao et al. (2022). ii) method. CAE v2 proposes visible and masked latent alignment to directly optimize the encoder and the regressor, respectively. Differently, MASKDISTILL and MVP supervise the overall model without separation. iii) loss type. Based on differences of the overall pipeline, different loss types perform inconsistent for achieving the best results. In detail, CAE v2 and MVP employ the cosine distance, while MASKDISTILL uses Smooth-ℓ_1.

4 Related Work

Masked image modeling (MIM) aims to learn transferable vision representations for various downstream tasks. It is inspired by the successful large-scale pretraining for transformers (Vaswani et al., 2017) with masked language modeling (MLM) (Devlin et al., 2019; Chen et al., 2020a; Brown et al., 2020; Dong et al., 2019) in NLP and can serve as a pretext task in self-supervised vision pretraining (Caron et al., 2018; Doersch et al., 2015; Oord et al., 2018; Ermolov et al., 2021; Goyal et al., 2021; Li et al., 2021; Zbontar et al., 2021; He et al., 2020; Chen et al., 2020c;b; Grill et al., 2020; Liu et al., 2022a; Dong et al., 2022; Zhang et al.,

2023; Huang et al., 2022a; Zhou et al., 2022b; Assran et al., 2022; Yi et al., 2023; Li et al., 2022). MIM methods (Bao et al., 2022; He et al., 2022; Xie et al., 2022; Chen et al., 2022a; Baevski et al., 2022; Singh et al., 2022; Peng et al., 2022a; Fang et al., 2023b;a; Peng et al., 2022b; Liu et al., 2022b; Singh et al., 2023) follow a mask-then-predict pipeline of (i) corrupting an image by masking several image patches based on a pre-defined mask ratio and then (ii) learning to predict the missing content under specific targets as a reconstruction task. Our CAE v2 follows this pipeline while using more semantic targets and incorporating two alignment losses to effectively facilitate model convergence and improve the encoder's representative ability. In the following, we will discuss the related works.

Targets. Existing MIM methods explore different kinds of targets within their frameworks, including RGB pixels (He et al., 2022; Gao et al., 2022), hand-crafted features like HOG descriptors (Wei et al., 2022a), discrete visual tokens (Bao et al., 2022; Chen et al., 2022a; El-Nouby et al., 2021; Peng et al., 2022a; Dong et al., 2021), and feature representations from momentum models (Tao et al., 2022; Chen et al., 2022b; Wu et al., 2023) or from external pre-trained models (Wei et al., 2022a;b; Liu et al., 2022b; Peng et al., 2022b; Fang et al., 2023b;a; Gao et al., 2023; Ren et al., 2023). Among these methods, the features from the vision branch of CLIP model play a significant role as supervision signals, substantially improving the following downstream task performance (Wei et al., 2022b; Liu et al., 2022b; Peng et al., 2022b; Fang et al., 2023b;a; Gao et al., 2023; Ren et al., 2023; Hou et al., 2022; Ren et al., 2023). The underlying reason is that CLIP latents can provide multi-modality knowledge to aid vision-only MIM learning, which is beneficial for improving the ability of the encoder that is used for downstream tasks. In our CAE v2, we also use CLIP latents as the target for the model pretraining. Meanwhile, we go further one step to tap the potential of CLIP latent to further improve the quality of the encoder via the following introduced alignment losses.

Loss function. Most literature (Wei et al., 2022a; He et al., 2022; Chen et al., 2022a; Bao et al., 2022; Peng et al., 2022a;b; Fang et al., 2023b;a; Ren et al., 2023; Liu et al., 2022b) apply the optimization to the predicted masked patches for the the masked patch prediction task. Following these methods, we also utilize a loss function for masked patch prediction task, which is called *masked latent alignment* since the optimization is applied to the representations of masked patches from the regressor. Furthermore, we find that directly applying supervision on the latent representations of visible patches from the encoder can constantly improve the model convergence and downstream transferring performance. We refer to this loss as *visible latent alignment*. Both visible and masked latent alignment use CLIP latent as the supervision target. In this way, the encoder can directly learn the semantic information from the powerful CLIP model, showing fast model convergence and high-quality encoder.

The most similar work to our approach is CAE (Chen et al., 2022a). Our CAE v2 is an improved variant of CAE, yet there is no decoder. Meanwhile, both visible latent alignment and masked latent alignment are conducted on the latent representations that need to be similar to those from the feature space of CLIP model. Instead, CAE contains a decoder to recover the predicted masked representations to the discrete tokens, and align the predicted representations of the masked patches to the encoded representation space.

In addition, several concurrent works also attempt to explore the potential of CLIP latents (Wei et al., 2022b; Peng et al., 2022a;b; Fang et al., 2023b;a; Ren et al., 2023; Liu et al., 2022b). For example, MILAN (Hou et al., 2022) focuses on the architecture design, dBOT (Liu et al., 2022b) proposes a training strategy, and MASKDISTILL (Peng et al., 2022b) carefully studies optimization methods. FD-CLIP (Wei et al., 2022c) aims to improve the CLIP model with CLIP latent using feature distillation on intact image patches, which is not a MIM-based method. It is worth noting that our CAE v2 is orthogonal to these works. Specifically, we concentrate on tapping the potential of CLIP latent, and present CAE v2 with visible latent alignment and masked latent alignment that both use CLIP latent as the pretraining target, which is beneficial for learning a high-quality encoder and facilitating model convergence. The proposed CAE v2 demonstrates that the explicit visible latent alignment is beneficial for the representation learning of the encoder. Moreover, we experimentally explore the relationship between the mask ratio and the model size. We hope our findings can provide valuable guidelines for the future MIM pretraining.

5 Conclusion and Limitation

This paper introduces CAE v2, a context autoencoder with CLIP latent alignment, using the latent features from the vision branch of CLIP as the supervision target. CAE v2 consists of two alignment losses, *i.e.*, visible latent alignment loss - on the representations of visible patches from the encoder, and masked latent alignment loss - on the predicted representations of masked patches from the regressor. Extensive analyses and experiments show that our CAE v2 effectively facilities model convergence and achieves high performance on various downstream vision tasks. CAE v2 also outperforms the CLIP vision encoder on these tasks, although CAE v2 is not designed for direct comparison with CLIP..

Limitation. Limited by resources, we do not examine larger models, such as ViT-Huge and ViT-Giant. We plan to explore this in the future and hope that the findings in CAE v2 will provide valuable guidance.

References

Mahmoud Assran, Mathilde Caron, Ishan Misra, Piotr Bojanowski, Florian Bordes, Pascal Vincent, Armand Joulin, Mike Rabbat, and Nicolas Ballas. Masked siamese networks for label-efficient learning. In *ECCV*, pp. 456–473, 2022.

Alexei Baevski, Wei-Ning Hsu, Qiantong Xu, Arun Babu, Jiatao Gu, and Michael Auli. Data2vec: A general framework for self-supervised learning in speech, vision and language. In *ICML*, pp. 1298–1312, 2022.

Hangbo Bao, Li Dong, Songhao Piao, and Furu Wei. BEit: BERT pre-training of image transformers. In *ICLR*, 2022.

Tom Brown, Benjamin Mann, Nick Ryder, Melanie Subbiah, Jared D Kaplan, Prafulla Dhariwal, Arvind Neelakantan, Pranav Shyam, Girish Sastry, Amanda Askell, et al. Language models are few-shot learners. *NIPS*, 33:1877–1901, 2020.

Zhaowei Cai and Nuno Vasconcelos. Cascade r-cnn: Delving into high quality object detection. In *CVPR*, pp. 6154–6162, 2018.

Mathilde Caron, Piotr Bojanowski, Armand Joulin, and Matthijs Douze. Deep clustering for unsupervised learning of visual features. In *ECCV*, pp. 132–149, 2018.

Mathilde Caron, Hugo Touvron, Ishan Misra, Hervé Jégou, Julien Mairal, Piotr Bojanowski, and Armand Joulin. Emerging properties in self-supervised vision transformers. In *ICCV*, pp. 9650–9660, 2021.

Mark Chen, Alec Radford, Rewon Child, Jeffrey Wu, Heewoo Jun, David Luan, and Ilya Sutskever. Generative pretraining from pixels. In *ICML*, pp. 1691–1703, 2020a.

Ting Chen, Simon Kornblith, Mohammad Norouzi, and Geoffrey Hinton. A simple framework for contrastive learning of visual representations. In *ICML*, pp. 1597–1607, 2020b.

Xiaokang Chen, Mingyu Ding, Xiaodi Wang, Ying Xin, Shentong Mo, Yunhao Wang, Shumin Han, Ping Luo, Gang Zeng, and Jingdong Wang. Context autoencoder for self-supervised representation learning. *arXiv preprint arXiv:2202.03026*, 2022a.

Xinlei Chen, Haoqi Fan, Ross Girshick, and Kaiming He. Improved baselines with momentum contrastive learning. *preprint arXiv:2003.04297*, 2020c.

Xinlei Chen, Saining Xie, and Kaiming He. An empirical study of training self-supervised vision transformers. In *ICCV*, pp. 9640–9649, 2021.

Yabo Chen, Yuchen Liu, Dongsheng Jiang, Xiaopeng Zhang, Wenrui Dai, Hongkai Xiong, and Qi Tian. Sdae: Self-distillated masked autoencoder. In *ECCV*, pp. 108–124, 2022b.

Kevin Clark, Minh-Thang Luong, Quoc V Le, and Christopher D Manning. Electra: Pre-training text encoders as discriminators rather than generators. In *ICLR*, 2020.

Jia Deng, Wei Dong, Richard Socher, Li-Jia Li, Kai Li, and Li Fei-Fei. Imagenet: A large-scale hierarchical image database. In *CVPR*, pp. 248–255, 2009.

Jacob Devlin, Ming-Wei Chang, Kenton Lee, and Kristina Toutanova. BERT: pre-training of deep bidirectional transformers for language understanding. In *NAACL*, pp. 4171–4186, 2019.

Carl Doersch, Abhinav Gupta, and Alexei A Efros. Unsupervised visual representation learning by context prediction. In *ICCV*, pp. 1422–1430, 2015.

Li Dong, Nan Yang, Wenhui Wang, Furu Wei, Xiaodong Liu, Yu Wang, Jianfeng Gao, Ming Zhou, and Hsiao-Wuen Hon. Unified language model pre-training for natural language understanding and generation. *NeurIPS*, 32, 2019.

Xiaoyi Dong, Jianmin Bao, Ting Zhang, Dongdong Chen, Weiming Zhang, Lu Yuan, Dong Chen, Fang Wen, and Nenghai Yu. Peco: Perceptual codebook for bert pre-training of vision transformers. *arXiv preprint arXiv:2111.12710*, 2021.

Xiaoyi Dong, Jianmin Bao, Ting Zhang, Dongdong Chen, Weiming Zhang, Lu Yuan, Dong Chen, Fang Wen, and Nenghai Yu. Bootstrapped masked autoencoders for vision bert pretraining. In *ECCV*, pp. 247–264, 2022.

Xiaoyi Dong, Yinglin Zheng, Jianmin Bao, Ting Zhang, Dongdong Chen, Hao Yang, Ming Zeng, Weiming Zhang, Lu Yuan, Wen Fang Chen, Dong, and Yu Nenghai. Maskclip: Masked self-distillation advances contrastive language-image pretraining. In *CVPR*, 2023.

Alexey Dosovitskiy, Lucas Beyer, Alexander Kolesnikov, Dirk Weissenborn, Xiaohua Zhai, Thomas Unterthiner, Mostafa Dehghani, Matthias Minderer, Georg Heigold, Sylvain Gelly, et al. An image is worth 16x16 words: Transformers for image recognition at scale. In *ICLR*, 2021.

Alaaeldin El-Nouby, Gautier Izacard, Hugo Touvron, Ivan Laptev, Hervé Jegou, and Edouard Grave. Are large-scale datasets necessary for self-supervised pre-training? *arXiv preprint arXiv:2112.10740*, 2021.

Aleksandr Ermolov, Aliaksandr Siarohin, Enver Sangineto, and Nicu Sebe. Whitening for self-supervised representation learning. In *ICML*, pp. 3015–3024, 2021.

Yuxin Fang, Quan Sun, Xinggang Wang, Tiejun Huang, Xinlong Wang, and Yue Cao. Eva-02: A visual representation for neon genesis. *arXiv preprint arXiv:2303.11331*, 2023a.

Yuxin Fang, Wen Wang, Binhui Xie, Quan Sun, Ledell Wu, Xinggang Wang, Tiejun Huang, Xinlong Wang, and Yue Cao. Eva: Exploring the limits of masked visual representation learning at scale. In *CVPR*, 2023b.

Peng Gao, Teli Ma, Hongsheng Li, Ziyi Lin, Jifeng Dai, and Yu Qiao. MCMAE: Masked convolution meets masked autoencoders. In *NIPS*, 2022.

Peng Gao, Renrui Zhang, Rongyao Fang, Ziyi Lin, Hongyang Li, Hongsheng Li, and Qiao Yu. Mimic before reconstruct: Enhancing masked autoencoders with feature mimicking. *arXiv preprint arXiv:2303.05475*, 2023.

Priya Goyal, Piotr Dollár, Ross Girshick, Pieter Noordhuis, Lukasz Wesolowski, Aapo Kyrola, Andrew Tulloch, Yangqing Jia, and Kaiming He. Accurate, large minibatch sgd: Training imagenet in 1 hour. *preprint arXiv:1706.02677*, 2017.

Priya Goyal, Mathilde Caron, Benjamin Lefaudeux, Min Xu, Pengchao Wang, Vivek Pai, Mannat Singh, Vitaliy Liptchinsky, Ishan Misra, Armand Joulin, et al. Self-supervised pretraining of visual features in the wild. *preprint arXiv:2103.01988*, 2021.

Jean-Bastien Grill, Florian Strub, Florent Altché, Corentin Tallec, Pierre H Richemond, Elena Buchatskaya, Carl Doersch, Bernardo Avila Pires, Zhaohan Daniel Guo, Mohammad Gheshlaghi Azar, Bilal Piot, Koray Kavukcuoglu, Rémi Munos, and Michal Valko. Bootstrap your own latent: A new approach to self-supervised learning. In *NeurIPS*, 2020.

Kaiming He, Georgia Gkioxari, Piotr Dollár, and Ross Girshick. Mask r-cnn. In *ICCV*, 2017.

Kaiming He, Haoqi Fan, Yuxin Wu, Saining Xie, and Ross Girshick. Momentum contrast for unsupervised visual representation learning. In *CVPR*, 2020.

Kaiming He, Xinlei Chen, Saining Xie, Yanghao Li, Piotr Dollár, and Ross Girshick. Masked autoencoders are scalable vision learners. In *CVPR*, pp. 16000–16009, 2022.

Zejiang Hou, Fei Sun, Yen-Kuang Chen, Yuan Xie, and S. Y. Kung. Milan: Masked image pretraining on language assisted representation. *ArXiv*, abs/2208.06049, 2022.

Gao Huang, Yu Sun, Zhuang Liu, Daniel Sedra, and Kilian Q. Weinberger. Deep networks with stochastic depth. In *ECCV*, 2016.

Lang Huang, Shan You, Mingkai Zheng, Fei Wang, Chen Qian, and Toshihiko Yamasaki. Green hierarchical vision transformer for masked image modeling. *arXiv preprint arXiv:2205.13515*, 2022a.

Zhicheng Huang, Xiaojie Jin, Chengze Lu, Qibin Hou, Ming-Ming Cheng, Dongmei Fu, Xiaohui Shen, and Jiashi Feng. Contrastive masked autoencoders are stronger vision learners. *arXiv preprint arXiv:2207.13532*, 2022b.

Sergey Ioffe and Christian Szegedy. Batch normalization: Accelerating deep network training by reducing internal covariate shift. In *ICML*, 2015.

Junnan Li, Pan Zhou, Caiming Xiong, and Steven Hoi. Prototypical contrastive learning of unsupervised representations. In *ICLR*, 2021.

Xiaotong Li, Yixiao Ge, Kun Yi, Zixuan Hu, Ying Shan, and Ling yu Duan. mc-beit: Multi-choice discretization for image bert pre-training. In *ECCV*, 2022.

Tsung-Yi Lin, Michael Maire, Serge Belongie, James Hays, Pietro Perona, Deva Ramanan, Piotr Dollár, and C Lawrence Zitnick. Microsoft coco: Common objects in context. In *ECCV*, pp. 740–755, 2014.

Hao Liu, Xinghua Jiang, Xin Li, Antai Guo, Deqiang Jiang, and Bo Ren. The devil is in the frequency: Geminated gestalt autoencoder for self-supervised visual pre-training. *arXiv preprint arXiv:2204.08227*, 2022a.

Xingbin Liu, Jinghao Zhou, Tao Kong, Xianming Lin, and Rongrong Ji. Exploring target representations for masked autoencoders. *arXiv preprint arXiv:2209.03917*, 2022b.

Ilya Loshchilov and Frank Hutter. Sgdr: Stochastic gradient descent with warm restarts. In *ICLR*, 2017.

Ilya Loshchilov and Frank Hutter. Decoupled weight decay regularization. In *ICLR*, 2019.

Aaron van den Oord, Yazhe Li, and Oriol Vinyals. Representation learning with contrastive predictive coding. *arXiv preprint arXiv:1807.03748*, 2018.

Zhiliang Peng, Li Dong, Hangbo Bao, Qixiang Ye, and Furu Wei. Beit v2: Masked image modeling with vector-quantized visual tokenizers. *arXiv preprint arXiv:2208.06366*, 2022a.

Zhiliang Peng, Li Dong, Hangbo Bao, Qixiang Ye, and Furu Wei. A unified view of masked image modeling. *TMLR*, 2022b.

Alec Radford, Jong Wook Kim, Chris Hallacy, Aditya Ramesh, Gabriel Goh, Sandhini Agarwal, Girish Sastry, Amanda Askell, Pamela Mishkin, Jack Clark, Gretchen Krueger, and Ilya Sutskever. Learning transferable visual models from natural language supervision. In *ICML*, 2021.

Colin Raffel, Noam Shazeer, Adam Roberts, Katherine Lee, Sharan Narang, Michael Matena, Yanqi Zhou, Wei Li, and Peter J Liu. Exploring the limits of transfer learning with a unified text-to-text transformer. *JMLR*, pp. 5485–5551, 2020.

Sucheng Ren, Fangyun Wei, Samuel Albanie, Zheng Zhang, and Han Hu. Deepmim: Deep supervision for masked image modeling. *arXiv preprint arXiv:2303.08817*, 2023.

Mannat Singh, Laura Gustafson, Aaron Adcock, Vinicius de Freitas Reis, Buğra Gedik, Raj Prateek Kosaraju, Dhruv Kumar Mahajan, Ross B. Girshick, Piotr Doll'ar, and Laurens van der Maaten. Revisiting weakly supervised pre-training of visual perception models. In *CVPR*, pp. 794–804, 2022.

Mannat Singh, Quentin Duval, Kalyan Vasudev Alwala, Haoqi Fan, Vaibhav Aggarwal, Aaron Adcock, Armand Joulin, Piotr Dollár, Christoph Feichtenhofer, Ross Girshick, et al. The effectiveness of mae pre-pretraining for billion-scale pretraining. *arXiv preprint arXiv:2303.13496*, 2023.

Jianlin Su, Yu Lu, Shengfeng Pan, Ahmed Murtadha, Bo Wen, and Yunfeng Liu. Roformer: Enhanced transformer with rotary position embedding. *arXiv preprint arXiv:2104.09864*, 2021.

Christian Szegedy, Vincent Vanhoucke, Sergey Ioffe, Jonathon Shlens, and Zbigniew Wojna. Rethinking the inception architecture for computer vision. In *CVPR*, 2016.

Chenxin Tao, Xizhou Zhu, Gao Huang, Yu Qiao, Xiaogang Wang, and Jifeng Dai. Siamese image modeling for self-supervised vision representation learning. *arXiv preprint arXiv:2206.01204*, 2022.

Hugo Touvron, Matthieu Cord, Matthijs Douze, Francisco Massa, Alexandre Sablayrolles, and Herv'e J'egou. Training data-efficient image transformers & distillation through attention. In *ICML*, pp. 10347–10357, 2021.

Ashish Vaswani, Noam Shazeer, Niki Parmar, Jakob Uszkoreit, Llion Jones, Aidan N Gomez, Łukasz Kaiser, and Illia Polosukhin. Attention is all you need. *NeurIPS*, 2017.

Shaoru Wang, Jin Gao, Zeming Li, Jian Sun, and Weiming Hu. A closer look at self-supervised lightweight vision transformers. *arXiv preprint arXiv:2205.14443*, 2022.

Chen Wei, Haoqi Fan, Saining Xie, Chao-Yuan Wu, Alan Yuille, and Christoph Feichtenhofer. Masked feature prediction for self-supervised visual pre-training. In *CVPR*, pp. 14668–14678, 2022a.

Huang Wei, Zhiliang Peng, Li Dong, Furu Wei, Jianbin Jiao, and Qixiang Ye. Generic-to-specific distillation of masked autoencoders. *arXiv preprint arXiv:2302.14771*, 2023.

Longhui Wei, Lingxi Xie, Wengang Zhou, Houqiang Li, and Qi Tian. Mvp: Multimodality-guided visual pre-training. *ECCV*, 2022b.

Yixuan Wei, Han Hu, Zhenda Xie, Zheng Zhang, Yue Cao, Jianmin Bao, Dong Chen, and Baining Guo. Contrastive learning rivals masked image modeling in fine-tuning via feature distillation. *arXiv preprint arXiv:2205.14141*, 2022c.

Zhirong Wu, Zihang Lai, Xiao Sun, and Stephen Lin. Extreme masking for learning instance and distributed visual representations. *TMLR*, 2023.

Tete Xiao, Yingcheng Liu, Bolei Zhou, Yuning Jiang, and Jian Sun. Unified perceptual parsing for scene understanding. In *ECCV*, pp. 418–434, 2018.

Zhenda Xie, Zheng Zhang, Yue Cao, Yutong Lin, Jianmin Bao, Zhuliang Yao, Qi Dai, and Han Hu. Simmim: A simple framework for masked image modeling. In *CVPR*, pp. 9653–9663, 2022.

Kun Yi, Yixiao Ge, Xiaotong Li, Shusheng Yang, Dian Li, Jianping Wu, Ying Shan, and Xiaohu Qie. Masked image modeling with denoising contrast. In *ICLR*, 2023.

Yang You, Igor Gitman, and Boris Ginsburg. Large batch training of convolutional networks. *preprint arXiv:1708.03888*, 2017.

Sangdoo Yun, Dongyoon Han, Seong Joon Oh, Sanghyuk Chun, Junsuk Choe, and Youngjoon Yoo. Cutmix: Regularization strategy to train strong classifiers with localizable features. In *ICCV*, pp. 6023–6032, 2019.

Jure Zbontar, Li Jing, Ishan Misra, Yann LeCun, and Stéphane Deny. Barlow twins: Self-supervised learning via redundancy reduction. In *ICML*, pp. 12310–12320, 2021.

Hongyi Zhang, Moustapha Cisse, Yann N. Dauphin, and David Lopez-Paz. mixup: Beyond empirical risk minimization. In *ICLR*, 2018.

Xiaosong Zhang, Yunjie Tian, Lingxi Xie, Wei Huang, Qi Dai, Qixiang Ye, and Qi Tian. Hivit: A simpler and more efficient design of hierarchical vision transformer. In *ICLR*, 2023.

Bolei Zhou, Hang Zhao, Xavier Puig, Sanja Fidler, Adela Barriuso, and Antonio Torralba. Scene parsing through ade20k dataset. In *CVPR*, pp. 633–641, 2017.

Jinghao Zhou, Chen Wei, Huiyu Wang, Wei Shen, Cihang Xie, Alan Yuille, and Tao Kong. ibot: Image BERT pre-training with online tokenizer. In *ICLR*, 2022a.

Qiang Zhou, Chaohui Yu, Hao Luo, Zhibin Wang, and Hao Li. Mimco: Masked image modeling pre-training with contrastive teacher. In *ACMMM*, pp. 4487–4495, 2022b.

A Appendix

B Implementation Details

B.1 Model structures

Encoder. For ViT-Tiny, we follow Wang et al. (2022) to increase the number of heads from 3 to 12. All others remain the same as the standard ViT architecture (Dosovitskiy et al., 2021). The end of encoder is a fully-connected layer (FC) followed by a layer normalization layer (LN) to map the target dimension to 512 for CLIP-Base and 768 for CLIP-Large. Note that FC and LN are discarded during the fine-tuning on downstream tasks.

Regressor. The regressor in CAE v2 is a stack of cross-attention based transformer blocks. For ViT-Tiny/-Small/-Base/-Large, we set the depth of regressor to 1/1/4/4, and the width to 96/384/768/1024. We also add a FC-LN after the regressor to map the target dimension, and these two layers share the same parameters to those in the encoder.

Targets. The targets in CAE v2 are derived from the last layer of the vision branch of CLIP model (Radford et al., 2021)[2], *i.e.*, the output of the projection head in the CLIP model with the dimension being 512 for CLIP-Base and 768 for CLIP-Large.

B.2 Pipeline Comparison

We compare the computational graphs for (a) our CAE v2, (b) CAE (Chen et al., 2022a), (c) BEiT (Bao et al., 2022), and (d) MAE (He et al., 2022) in Figure 5. The key novelty of CAE v2 is visible latent alignment and masked latent alignment, which are directly optimize the feature space of the encoder and regressor to be close to CLIP latents.

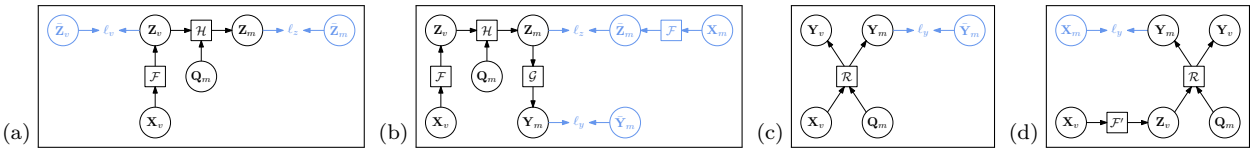

Figure 5: The computational graphs for (a) our CAE v2, (b) CAE (Chen et al., 2022a), (c) BEiT (Bao et al., 2022), and (d) MAE (He et al., 2022). The parts in cornflower blue are for loss function. The encoder in (a) and (b) receives the visible patches and outputs their latent representations. The regressor predicts masked latent representations. (a) Visible latent alignment is applied on the representation learning of the encoder, and masked latent alignment loss is for predicting representations of masked patches. (b) The decoder reconstructs the masked patches from masked latent representations. (c) The input includes both visible patches and mask queries, and the representations for them are updated within the function $\mathcal{R}$. (d) The encoder $\mathcal{F}^{'}$ only processes the visible patches $\mathbf{X}_v$, and the decoder $\mathcal{R}$ inputs both latent representations and mask queries. For simplicity, the positional embeddings are not included in computational graphs.

B.3 Training Details

pretraining. We present the default pretraining settings in Table 8. The pretraining epoch for all experiments is 300. For the CLIP model, we use base-size model for ViT-Tiny/-Small/-Base and the large-size model for ViT-Large. The input size is 224×224 for CLIP-Base and 196×196 for CLIP-Large. The input images are the same as those in the backbone model. We only use ImageNet-1K (Deng et al., 2009) for pretraining.

Linear Probing on ImageNet-1K (Deng et al., 2009). Following He et al. (2022); Doersch et al. (2015), we adopt an extra batch normalization layer (Ioffe & Szegedy, 2015) without affine transformation after the encoder. The default training details are shown in Table 9.

[2]The official pretrained CLIP model is available at `https://github.com/openai/CLIP/blob/main/clip/clip.py`.

Table 8: **pretraining setting** for CAE v2 on ImageNet-1K.

Config	Value
	ViT-Tiny/Small/Base/Large
Optimizer	AdamW (Loshchilov & Hutter, 2019)
Peak learning rate	1.5e-3
Minimal learning rate	1e-5
Optimizer momentum	β_1, β_2=0.9, 0.98 (Chen et al., 2020a)
Batch size	2048
Learning rate schedule	Cosine decay (Loshchilov & Hutter, 2017)
Warmup epochs (Goyal et al., 2017)	10
Max training epochs	300
Gradient Clipping	3.0
Weight decay	0.05
Drop path	0.1/0.1/0.1/0.2
Mask ratio	0.15/0.25/0.5/0.6
Mask strategy	Random block-wise sampling
Input scale	min=0.4, max=1.0
Data Augmentation	Random resized crop & horizontal flip
Color jitter	0.4
Input size	224×224

Table 9: **Linear probing setting** for CAE v2 on ImageNet-1K.

Config	Value
	ViT-Tiny/Small/Base/Large
Optimizer	LARS (You et al., 2017)
Base learning rate	0.1
Weight decay	0
Optimizer momentum	0.9
Batch size	16384
Warmup epochs	10
Max training epochs	90
Data augmentation	Random resized crop & horizontal flip

Fine-tuning on ImageNet-1K (Deng et al., 2009). The default settings for ImageNet-1K fine-tuning are in Table 10. The fine-tuning epoch for ViT-Tiny/-Small/-Base/-Large is 100/200/100/50 for fair comparison. The input size of all scales of models is 224×224. For ViT-Tiny, we sweep the learning rate ranging from 1e-3 to 4e-3. For ViT-Small/Base/Large, we select the learning rate from 1e-4 to 5e-4. By default, the learning rates and the layer-wise lr decay are 2e-3/5e-4/2e-4/4e-4 and 0.75/0.8/0.75/0.8 for ViT-Tiny/Small/Base/Large, respectively.

Semantic segmentation in ADE20K (Zhou et al., 2017). We follow the common setting in BEiT (Bao et al., 2022) to use UperNet (Xiao et al., 2018) as the task head and report the mIoU on ADE20K (Zhou et al., 2017). We add relative position bias (Raffel et al., 2020) during fine-tuning. For different scales of models in CAE v2, we search for the optimal learning rate and layer-wise learning rate decay in Table 11 for Table 6 in the main paper. Specifically, we select the optimal learning rate from {8e-5, 1e-4, 1.5e-4, 2e-4} for ViT-Tiny/Small/Base and from {1e-5, 2e-5, 3e-5, 4e-5} for ViT-Large.

Object detection and instance segmentation in COCO (Lin et al., 2014). We use COCO (Lin et al., 2014) for the evaluation on object detection and instance segmentation. We adopt both Mask R-CNN (He et al., 2017) and Cascade Mask R-CNN (Cai & Vasconcelos, 2018) frameworks and report AP^b and AP^m on the COCO val split. The input image is resized with the size of the short side between 480 and 800, while the size of the long side is no larger than 1333. Meanwhile, we use the relative position embedding and rotary position embedding (Su et al., 2021) during pretraining. Other training details are shown in Table 12.

Table 10: **Fine-tuning setting** for CAE v2 on ImageNet-1K.

Config	Value
	ViT-Tiny/Small/Base/Large
Optimizer	AdamW (Loshchilov & Hutter, 2019)
Peak learning rate	{1, 2, 3, 4}e-3/ {1, 2, 3, 4, 5}e-4
Minimal learning rate	1e-6
Weight decay	0.05
Optimizer momentum	β_1, β_2=0.9, 0.999 (Chen et al., 2020a)
Layer-wise lr decay (Bao et al., 2022; Clark et al., 2020)	{0.75, 0.8}
Batch size	1024
Learning rate schedule	Cosine decay (Loshchilov & Hutter, 2017)
Warmup epochs (Goyal et al., 2017)	5
Max training epochs	100/100/100/50
Data Augmentation	RandAug(10/9/9/9,0.5)
Label smoothing (Szegedy et al., 2016)	0.0/0.1/0.1/0.1
Mixup (Zhang et al., 2018)	0.2/0.8/0.8/0.8
Cutmix (Yun et al., 2019)	0.0/1.0/1.0/1.0
Color jitter	0.3/0.4/0.4/0.4
Drop path (Huang et al., 2016)	0.0/0.1/0.1/0.2
Input size	224×224

Table 11: **Semantic segmentation setting** for CAE v2 on ADE20K.

Config	Value
	ViT-Tiny/Small/Base/Large
Optimizer	AdamW (Loshchilov & Hutter, 2019)
Peak learning rate	{0.8, 1, 1.5, 2}e-4/{1, 2, 3, 4}e-5
Minimal learning rate	1e-6
Weight decay	0.05
Optimizer momentum	β_1, β_2=0.9, 0.999 (Chen et al., 2020a)
Layer-wise lr decay (Bao et al., 2022; Clark et al., 2020)	{0.65, 0.75, 0.8, 0.85, 0.95}
Batch size	16
Learning rate schedule	Polynomial decay
Warmup steps	1500
Max training steps	160000
Drop path (Huang et al., 2016)	0.1/0.1/0.1/0.15
Input size	512×512

Table 12: **Object detection and instance segmentation setting** for CAE v2 on COCO.

Config	Value
	ViT-Small/Base/Large
Optimizer	AdamW (Loshchilov & Hutter, 2019)
Peak learning rate	{1, 1.5, 2, 3, 4}e-4
Minimal learning rate	1e-6
Weight decay	0.05
Optimizer momentum	β_1, β_2=0.9, 0.999 (Chen et al., 2020a)
Layer-wise lr decay (Bao et al., 2022; Clark et al., 2020)	{0.8, 0.85, 0.95}
Batch size	16
Learning rate schedule	Step
Step epochs	8, 11
Max training epochs	12
Drop path (Huang et al., 2016)	0.2